Obstructive Sleep Apnea Affects Lacrimal Gland Function

Shaopan Wang,[1,2,8] Xin He,[1–3] Qingmin Li,[4] Yuhan Zhang,[1,2] Jiaoyue Hu,[1,2,5,6] Rongrong Zong,[1,2] Jingyi Zhuang,[3] Andrew J. Quantock,[7] Yingying Gao,[4] Wei Li,[1,2,5,6,] and Zuguo Liu[1,2,5,6,8]

[1]Eye Institute of Xiamen University, School of Medicine, Xiamen University, Xiamen, Fujian, China
[2]Fujian Provincial Key Laboratory of Ophthalmology and Visual Science, Xiamen University, Xiamen, Fujian, China
[3]Department of Ophthalmology, the First Affiliated Hospital of Xiamen University, Xiamen University, Xiamen, Fujian, China
[4]Department of Ophthalmology, the Second Affiliated Hospital, Fujian Medical University, Quanzhou, Fujian, China
[5]Department of Ophthalmology, Xiang'an Hospital of Xiamen University, Xiamen University, Xiamen, Fujian, China
[6]Xiamen University Affiliated Xiamen Eye Center, Xiamen University, Xiamen, Fujian, China
[7]School of Optometry and Vision Sciences, Cardiff University, Cardiff, Wales, United Kingdom
[8]Institute of Artificial Intelligence, Xiamen University, Xiamen, Fujian, China

Correspondence: Zuguo Liu, Eye Institute of Xiamen University, Chengyi Building, 4th Floor, 4221-122, South Xiang'an Rd, Xiamen, Fujian 361102, China; zuguoliu@xmu.edu.cn.
Wei Li, Eye Institute of Xiamen University, Chengyi Building, 4th Floor, 4221-122, South Xiang'an Rd, Xiamen, Fujian 361102, China; wei1018@xmu.edu.cn.
Ying-Ying Gao, Department of Ophthalmology, the Second Affiliated Hospital, Fujian Medical University, Quanzhou, Fujian, 362000, China; gaoyingying1968@163.com.

SW, XH, and QL contributed equally to this work thus should be considered as co-first authors.

Received: October 17, 2021
Accepted: February 12, 2022
Published: March 3, 2022

Citation: Wang S, He X, Li Q, et al. Obstructive sleep apnea affects lacrimal gland function. *Invest Ophthalmol Vis Sci.* 2022;63(3):3. https://doi.org/10.1167/iovs.63.3.3

Purpose. To determine the effect of obstructive sleep apnea syndrome (OSA) on lacrimal gland function and its mechanism.

Methods. Male mice aged seven to eight weeks were housed in cages with cyclic intermittent hypoxia to mimic OSA, and the control group was kept in a normal environment. Slit-lamp observation, fluorescein staining, and corneal sensitivity detection are used to assess cornea changes. Tear secretion was detected by phenol red cotton thread, and the pathological changes of lacrimal gland were observed by hematoxylin and eosin staining, oil red O staining, cholesterol and triglyceride kits, immunofluorescence staining, immunohistochemical staining, real-time polymerase chain reaction, transmission electron microscopy, and Western blot.

Results. Studies revealed a decreased tear secretion, corneal epithelial defects and corneal hypersensitivity. Myoepithelial cell damage, abnormal lipid accumulation, reduced cell proliferation, increased apoptosis and inflammatory cell infiltration in the lacrimal gland were also seen. *Hifα* and NF-κB signaling pathways, moreover, were activated, while *Pparα* was downregulated, in the lacrimal glands of OSA mice. Fenofibrate treatment significantly alleviated pathological changes of the lacrimal gland induced by OSA.

Conclusion. OSA disturbs the *Hifα*/*Pparα*/NF-κB signaling axis, which affects lacrimal gland structure and function and induces dry eye.

Keywords: Obstructive sleep apnea, lacrimal gland, dry eye, ocular surface

Sleep apnea is a disease characterized by airway obstruction or recurrent apnea during sleep owing to respiratory changes controlled by the central nervous system.[1] Obstructive sleep apnea (OSA) syndrome is recognized as a global public health disease. Approximately one billion people suffer from OSA,[2] and the prevalence of mild OSA can reach 84% in people over 65 years of age, comprising 90% of men and 78% of women.[3] Several studies have indicated the high cost of diagnosing and treating OSA,[4–7] with the disease placing a serious burden on individuals and society. OSA, moreover, is reportedly linked to numerous conditions such as cardiovascular disease,[8,9] diabetes,[10] depression,[11] male infertility,[12] stroke, and even death.[13] Simultaneously, OSA has been found to be associated with various ophthalmic diseases that include glaucoma,[14,15] floppy eyelid syndrome,[16] optic neuropathy,[17,18] and keratoconus.[19,20]

Dry eye is a multifactorial ocular surface disease caused by an imbalance in tear film homeostasis.[21] Its prevalence has been estimated at 5% to 50% with conspicuous variability, reaching 75% in some populations.[22] Recently, Karaca and associates[23] reported a shorter tear breakup time and decreased tear secretion in OSA patients, whereas Lim and colleagues[24] found that a high risk of sleep apnea is associated with symptoms of dry eye. Nevertheless, the possibility of a causative relationship between OSA and dry eye, and its likely mechanism, has yet to be established.

Copyright 2022 The Authors

This work is licensed under a Creative Commons Attribution-NonCommercial-NoDerivatives 4.0 International License.

Downloaded from intl.iovs.org on 04/19/2024

The lacrimal gland is a pivotal part of the ocular surface microenvironment.[25] It secretes aqueous tears to maintain the homeostasis of the ocular surface. The lacrimal gland can be prone to pathological changes owing to abnormal glucose metabolism[26] or lipid metabolism,[27] and lesions of the lacrimal gland are often accompanied by abnormal deposition of lipids with increasing age and when sleep deprived.[28,29] The current study suggests that OSA is a causative factor for dry eye disease and reveals a mechanism by which OSA could lead to abnormal lacrimal gland lipid metabolism through the *Hif-Pparα* signaling pathway, ultimately triggering manifestations of dry eye. We also report on the beneficial therapeutic effect of systemic fenofibrate for the treatment of OSA-induced lacrimal gland lesions.

Materials and Methods

Establishment of OSA Mice Model

Male C57BL/6J mice aged seven to eight weeks were purchased from the Shanghai SLAC Center (Shanghai, China). Animals were housed in ventilated cages with a room temperature of approximately 25°C and air humidity around 60%. Indoor light exposure was maintained from 8:00 a.m. to 8:00 p.m. The "chronic intermittent hypoxia" method is widely used to mimic OSA in experimental mice[30–32] and was used here. Briefly, after acclimating for one week, mice in the OSA group were placed in a custom-made cage, daily from 9:00 a.m. to 5:00 p.m. every day for four weeks. The oxygen concentration in the cage was caused to rise and fall periodically by the use of a controlled gas delivery system. The gas in the cage maintained a steady flow and was adjusted according to the following cycle: nitrogen infusion for 35 seconds followed by a 10-second pause; infusion of pure oxygen for 10 seconds; filling of the cage with air for 35 seconds (Fig. 1A). The oxygen concentration in the cage was monitored in real time using an oxygen concentration detector (BH-90A; Bosean, Henan, China). OSA mice were returned to a normal atmospheric environment at the end of the experimental period, with mice in the control group being housed throughout in a normal atmospheric environment. The treatment group was fed with 100 mg/kg/d of fenofibrate (Medison Bio-Pharmaceutical., Ltd., Jiangsu, China) during the experimental period. In total 110 mice were used in this study. They were randomly assigned to five groups of 22 mice each, and the number of animals applied in specific experiments were described in the figure legends. All experimental procedures were reviewed and approved by the Ethics Committee for Animal Experiments of Xiamen University, and all met the relevant requirements of the Association for Research in Vision and Ophthalmology.

Measurement of Mice Tear Production and Corneal Sensitivity

The tear secretion of mice was measured each day at 6:00 p.m. Accumulated tears in the conjunctival sac of the mice were blotted with aseptic filter paper without touching the eyeball. A phenol red cotton thread (Zone-Quick, Japan) was then placed, one-third of the distance away from the lateral canthus of the lower eyelid of the mouse for 15 seconds. The thread was then removed, and the tear production measured in millimeters. Corneal sensitivity was measured by a Cochet-Bonnet vibrometer (Western Ophthalmics, Lynnwood, WA, USA) as previously described.[28] Briefly, five consecutive vertical contacts with central cornea by tactile nylon filament were performed. Positive result was recorded if three blinking behaviors were induced out of five contacts. The filament of instrument was reduced each time by 1 cm from the full length to 6 cm, until the above positive result was obtained. The filament length is then recorded as corneal sensitivity result.

Hematoxylin & Eosin Staining

The lacrimal glands of mice were removed after the animals had been euthanized by cervical dislocation and fixed in 4% paraformaldehyde for 24 hours. They were then sequentially immersed in 70% ethanol, 80% ethanol, 95% ethanol, and 100% ethanol, embedded in paraffin and sectioned at 5 µm using a paraffin microtome. Sections were picked up on slides and after dewaxing with xylene and rehydrating with graded ethanol, were washed with phosphate buffered saline solution (PBS). Sections were stained with hematoxylin for five minutes and eosin solution for one minute, after which they were rinsed in running water for five minutes and placed into graded ethanol. After mounting, photographs were taken with a light microscope (Carl Zeiss Axio Lab.A1, Jena, Germany).

Oil Red O Staining

Frozen sections of the lacrimal glands were fixed with 4% paraformaldehyde for five minutes and subsequently rinsed with PBS. The sections were then stained with 0.5% oil red O dissolved in isopropanol for 15 minutes, followed by a wash with PBS. Tissue slides were further stained with hematoxylin for 15 seconds and rinsed with tap water for 10 minutes, after which they were dried and mounted with glycerol. The distribution of lipids was observed under a light microscope (Carl Zeiss Axio Lab.A1).

Immunofluorescence Staining

Frozen sections were fixed with 4% paraformaldehyde for 20 minutes. They were subsequently washed with PBS and covered with 0.2% Triton for 20 minutes, followed by blocking with 2% bovine serum albumin for one hour. CD45 (1:200, sc-25590; Santa Cruz Biotechnology, Dallas, TX, USA), F4/80 (1:200, 30325; Cell Signaling Technology, Danvers, MA, USA), TOM20 (1:200, 11802-1-AP; Proteintech, Rosemont, IL, USA), TIM23 (1:200, 11123-1-AP; Proteintech), α-smooth muscle actin (αSMA) (1:200, ab32575; Abcam, Cambridge, MA, USA) and Ki67 (1:200, ab16667; Abcam) antibodies were then added and sections incubated overnight at 4°C. After washing with PBS, the secondary antibody (1:300, Alexa Fluor 594 conjugated IgG, A21207 or Alexa Fluor 488 conjugated IgG, A21206; Invitrogen, Carlsbad, CA, USA) was added to the sections for one hour at room temperature. After washing with PBS, slides were mounted with DAPI as a nuclear stain. Sections were visualized and photographed using a Zeiss LSM 880 laser confocal microscope (Zeiss, Oberkochen, Germany).

Immunohistochemistry Staining

Paraffin sections were deparaffinized, rehydrated, and placed in an antigen retrieval solution consisting of 10 mmol/L sodium citrate and 0.05% Tween 20. After heating to boiling point in a microwave oven for 20 minutes,

Investigative Ophthalmology & Visual Science

Downloaded from intl.iovs.org on 04/19/2024

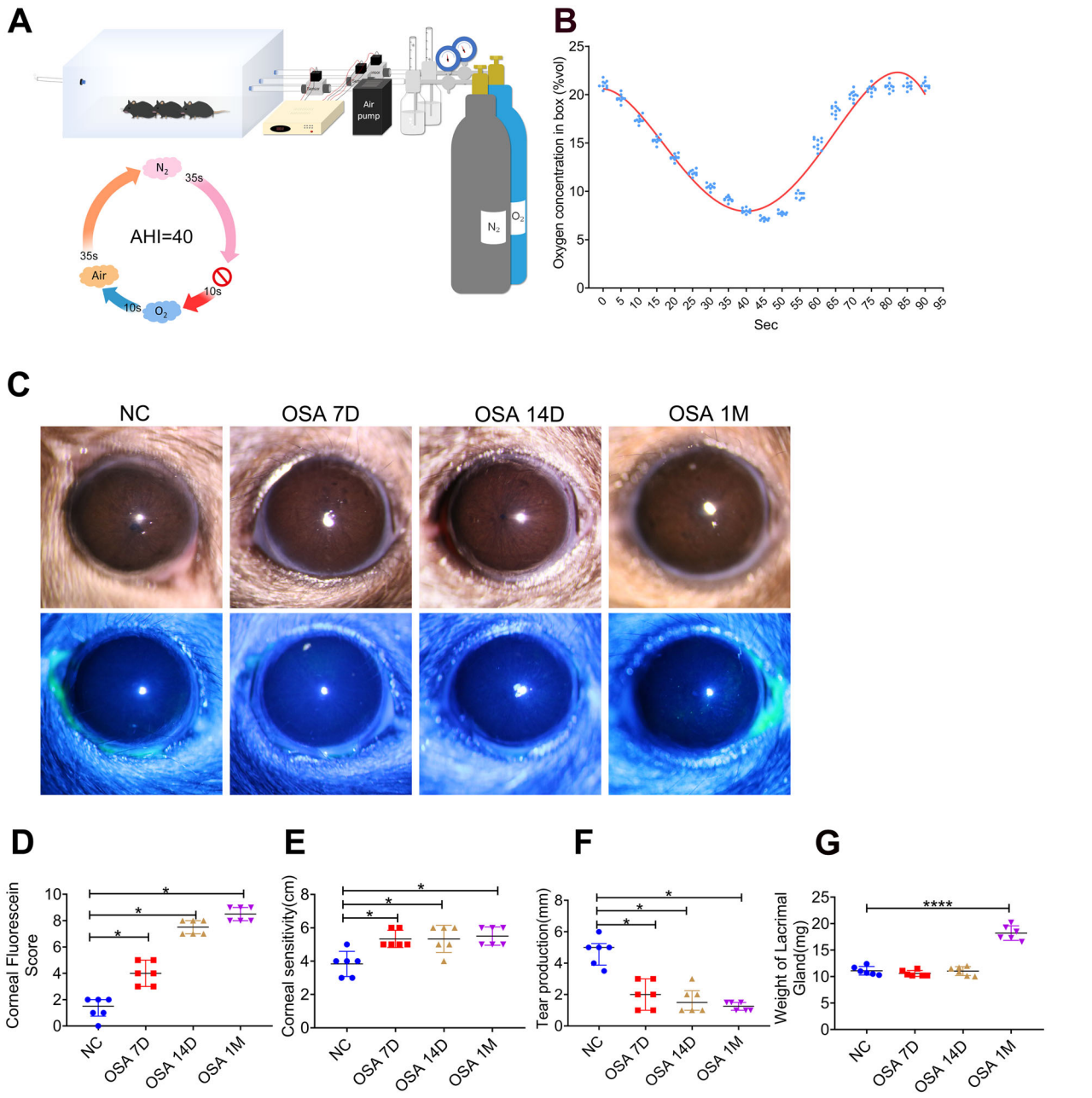

Figure 1. OSA induces dry eye changes in mice. (A) Schematic of the OSA induction protocol. (B) Oxygen concentration is monitored in real time over 90-second cycles. (C) Slit-lamp images and fluorescein staining of mouse corneas after different durations of OSA induction. (D) Fluorescein staining scores indicate corneal epithelial defects in OSA mice. (E) Corneal sensitivity increases in OSA mice. (F) Aqueous tear production decreases in OSA mice. (G) Lacrimal gland weight increases in mice induced with OSA for one month. n = 6 (C–G); n = 10 (B). *$P < 0.05$, ****$P < 0.0001$. D, day; M, month; NC, negative control; AHI, Apnea–Hypopnea Index.

slides were rinsed in tap water for 15 minutes. Specimens were then treated with 0.06% hydrogen peroxide for half an hour at room temperature, followed by incubation with 0.2% Triton for 20 minutes, washing with PBS, and blocking with 2% bovine serum albumin for one hour at room temperature. CD4 (1:1000, ab183685; Abcam), HIF1α (1:1000, ab2185; Abcam), and HIF2α (1:200, 49814; Signalway Antibody, Greenbelt, MD, USA) antibodies were then added, followed by an incubation overnight at 4°C. After three washes with PBS for 15 minutes, the secondary antibody (PV6001; ZSGB-BIO, Beijing, China) was added and the sections incubated for one hour. After washing with PBS, the reaction product was developed with diaminobenzidine chromogenic solution (ZLI9019; ZSGB-BIO) for one minute, mounted with mounting medium, and examined under a light microscope (Eclipse 50i; Nikon, Tokyo, Japan).

TUNEL Assay

A TUNEL assay was used to detect cell apoptosis in lacrimal glands. Frozen sections, after fixation, were treated with proteinase K for 10 minutes. Subsequently, negative and

Investigative Ophthalmology & Visual Science

Downloaded from intl.iovs.org on 04/19/2024

positive controls were treated with DNAase for 10 minutes each, followed by washes with PBS. Sections were then incubated with equilibration buffer for 10 minutes at room temperature, followed by reagent mix (DeadEnd Fluorometric TUNEL System G3250; Promega Corporation, Madison, WI, USA) at 37°C for one hour. Tissue specimens were then soaked in saline sodium citrate (DeadEnd Fluorometric TUNEL System, G329A; Promega) for 15 minutes. Slides were mounted with DAPI after washing three times with PBS and imaged with a LSM 880 confocal microscope (Zeiss).

Cholesterol and Triglyceride Detection Assay

Cholesterol and triglyceride kits (A111-1-1 and A110-1-1; Nanjing Jiancheng Bioengineering, Nanjing, China) were used to quantify cholesterol and triglyceride contents in the lacrimal gland and serum. After the mice were anesthetized by intraperitoneal injection of 1% pentobarbital sodium solution, blood was collected from the retro-orbital venous plexus, left to stand for one hour at 37°C and spun in a centrifuge for 10 minutes at 5000 rpm. The supernatant was then transferred to a new tube. Lacrimal gland tissues were homogenized in normal saline solution immediately after excision. In brief, we prepared homogenate by adding nine volumes of homogenization medium (0.86% normal saline solution) according to the ratio of lacrimal gland weight (g): volume (mL) = 1:9 according to the method of kit manufacturer. Centrifuging the prepared 10% homogenate at 2500 rpm for 10 minutes and taking the supernatant for determination of lipids content. Cholesterol and triglyceride content were calculated from absorbance values measured at a wavelength of 510 nm.

Transmission Electron Microscopy

Excised lacrimal glands were washed with PBS, cut into small blocks, and immersed in 2.5% glutaraldehyde in phosphate buffer overnight at 4°C. Samples were then washed with PBS and sodium cacodylate, respectively, and immersed in 1% OsO_4 solution for two hours. Each sample was subsequently partially dehydrated at room temperature by adding to solutions of 30% and then 50% ethanol, followed by staining with 70% uranyl acetate at 4°C for four hours. The dehydration was continued at room temperature with a concentration gradient of 70%, 90%, 100% ethanol for 15 minutes each immersion. Next, specimens were embedded in Spurr resin, after which ultrathin sections were cut at 75 nm with an ultramicrotome and picked up on copper grids and stained for 10 minutes with a 10% solution of lead citrate. Tissue sections were observed and photographed using a Hitachi HT-7800 transmission electron microscope (Hitachi, Tokyo, Japan).

Quantitative Real-time PCR

RNA from lacrimal gland tissue was extracted with cooled TRIzol reagent (10606ES60; YEASEN, Shanghai, China) and reverse transcribed into cDNA with a ExScript RT Reagent kit (Takara Bio, Kyoto, Japan). Quantitative real-time PCR (qRT-PCR) was performed by using a Step One system (Applied Biosystems, Foster City, CA, USA). The amplification program follows established procedures reported elsewhere.[27] Supplementary Table S1 lists the primer sequences used. The expression of genes was assessed by the $2^{-\Delta\Delta Ct}$ method.[33]

Western Blot Analysis

To determine relevant protein expression levels in lacrimal gland tissue, mice were sacrificed and the lacrimal glands subjected to protein extraction with RIPA buffer (R0278; Sigma-Aldrich Corp., St. Louis, MO, USA) and a protease inhibitor cocktail (1861281; Thermo Fisher Scientific, Waltham, MA, USA). Subsequently, electrophoresis was performed with 10% sodium dodecyl sulfate-polyacrylamide gels. After the end of the electrophoresis, the protein was transferred to polyvinylidene difluoride membrane (PVDF) membrane and blocked in 5% bovine serum albumin for two hours. The membranes were incubated with PPARα (1:1000, ab8934; Abcam), CPT1A (1:1000, ab220789; Abcam) , NRF2 (1:1000, 16396-1-AP; Proteintech), SOD2(1:1000, 24127-1-AP; Proteintech), total NF-κB P65 (1:1000, 8242s; Cell Signaling Technology) or Phospho-NF-κB P65 (1:1000, 3033s; Cell Signaling Technology) antibodies overnight on a shaker at 4°C. After washing three times for 10 minutes each with Tris-buffered saline containing 0.05% Tween-20 (TBST) solution, the membranes were incubated with horseradish peroxidase–conjugated secondary antibody (1:10000, Goat Anti-Rabbit IgG H&L; Abcam) for one hour. After washing three times with TBST solution, the results were visualized by enhanced chemiluminescence reagents (Advansta, San Jose, CA, USA), and the corresponding bands of the protein were obtained.

Statistical Analysis

Quantitative data from images was obtained using Image J software (Version 1.52; National Institutes of Health, Bethesda, MD, USA). In brief, the immunofluorescence images were transferred into gray scale, and the positive staining randomly selected at least three or more regions was analyzed by Image J software. Quantitative analysis of CD4 immunohistochemical staining was performed using the Immunohistochemical Profile module of Image J software. We took the sum of all positive percentages automatically obtained by this software as the final positive percentage, that is, final Positive percentage (%) = High Positive (%) + Positive (%) + Low Positive (%), then compared the final positive percentage between different groups. All the samples were photographed with the same exposure time in a confocal laser scanning microscope (Zeiss LSM 880, Zeiss). Each sample was examined with at least three different areas studied. Results were analyzed using software GraphPad Prism (Version 8.0.1; San Diego, CA, USA). We used Shapiro-Wilk normality test to analyze whether the data fit a normal distribution. The data that met the normal distribution were analyzed using a *t*-test or analysis of variance. The Wilcoxon rank sum test was performed to analyze the data that did not conform to the normal distribution. The error bars represent mean with standard deviation in normality distribution results or median and interquartile range in non-normality distribution groups. $P < .05$ was recognized as statistically significant.

Results

Symptoms of Dry Eye in the OSA Mouse Model

A mouse model of OSA was established that simulated 40 apneas per hour (Fig. 1A), representing an Apnea-Hypopnea Index of 40. The maximum oxygen concentration attained

Investigative Ophthalmology & Visual Science

Downloaded from intl.iovs.org on 04/19/2024

was approximately 21%, with the minimum oxygen concentration around 7.2% (Fig. 1B). After one month of OSA, there was no body weight increase in OSA group compared with 14 days. And the body weight was higher in normal control group, compared with OSA group (Supplementary Fig. S1). After seven days of OSA, corneal epithelial defects were evident in OSA mice based on fluorescein staining, which became more pronounced after one month (Figs. 1C, 1D). Corneal sensitivity began to increase after one week and remained at a relatively high level throughout the OSA period (Fig. 1E). Tear secretion in OSA mice decreased to about half of normal control levels after seven days and remained low until one month (Fig. 1F). The weight of the lacrimal glands in OSA mice was essentially unchanged at days seven and 14 but had increased significantly at the one-month timepoint (Fig. 1G). The ocular surface manifestations confirmed that after seven days of simulated OSA induction, the OSA mice had developed dry eye changes.

Abnormal Lipid Metabolism and Altered Mitochondrial Integrity in the Lacrimal Glands of OSA Mice

Previous studies in our laboratories discovered lipid accumulation in lacrimal glands of various dry eye syndrome animal models.[27,28] Here, oil red O staining disclosed a heightened deposition of lipid in lacrimal gland cells of seven-day OSA mice, which persisted and became more prominent at one month. In contrast, only a small amount of lipid was observed in normal lacrimal gland cells (Fig. 2A). Transmission electron microscopy revealed that a large number of lipid droplets had accumulated in acinar cells of the lacrimal glands of OSA mice (Fig. 2C). Oil red O staining disclosed no lipid deposition in liver cells of the OSA or control groups (Fig. 2D), indicating that the lacrimal gland is more susceptible than the liver to abnormal lipid deposition as a consequence of OSA. Cholesterol (Fig. 2E) and triglyceride (Fig. 2F) were also detected in lacrimal glands of OSA mice and were found to be increased significantly as early as day seven of OSA induction. Elevated levels were maintained until the one-month juncture. On the other hand, cholesterol (Fig. 2G) and triglyceride (Fig. 2H) levels in blood serum measured from day seven to one month were unchanged in the OSA group compared with the control group.

Peroxisome proliferator-activated receptor α (*Ppar*α) plays an important role in controlling the expression of multiple genes involved in lipid metabolic pathways, such as those involved with fatty acid oxidation, the synthesis and breakdown of triglycerides and lipid droplets, and lipoprotein metabolism.[34] To investigate whether the deposition of lipid droplets was accompanied with changes in lipid metabolism-related genes, *Ppar*α—carnitine palmitoyl transferase 1a (*Cpt1a*), fatty acid synthetase (*Fas*) and *Cd36*—was examined by qRT-PCR. *Cpt1a* catalyzes the transfer of a long-chain fatty acyl group from CoA to carnitine, and is involved in fatty acid transport and oxidation. *Fas* is integral to lipogenesis, whereas *Cd36* impacts on long-chain fatty acid metabolism and the oxidization of low-density lipid.[35] The results indicate that the expression of *Ppar*α decreases significantly at day seven of OSA and remains low until one month. *Cpt1a* gene expression was decreased at one month, whereas *Fas* and *Cd36* expression gradually increased from day seven to one month (Fig. 2I). Western blot analysis confirmed the decrease of PPARα and CPT1A expression in the lacrimal glands of OSA mice at one month (Figs. 2J–L).

Based on the notion that lipid accumulation in lacrimal gland acinar cells will cause lipid oxidation of mitochondria,[27] we performed TIM23 and TOM20 immunofluorescence staining to evaluate mitochondrial integrity. In seven-day OSA mice, expression of the translocase of the inner mitochondrial membrane TIM23 (Figs. 3A, 3B) and the translocase of the outer mitochondrial membrane TOM20 (Figs. 3C, 3D) were both reduced, with low levels maintained until one month. Transmission electron microscopy documented mitochondrial swelling after seven days of OSA, which persisted and increased with time (Fig. 3E).

Inflammatory and ROS Changes in the OSA Mouse Lacrimal Gland

In humans, OSA can induce persistent low-level inflammation,[36] so we investigated the inflammatory status in the lacrimal glands of OSA mice. Hematoxylin and eosin staining showed that cell infiltration had begun at day 7, becoming more noticeable at day 14, with infiltrated cells mainly located around blood vessels. After 1 month of OSA, multiple infiltration foci presented in single tissue sections (Fig. 4A). Immunohistochemical staining of mouse OSA lacrimal glands for CD4 revealed low, but increasing, levels of scattered lymphocyte infiltration at days 7 and 14, with clusters forming by 1 month (Fig. 4B and E). CD45 staining demonstrated significant leukocyte infiltration from day 7 (Figs. 4C, 4F), with F4/80-positive macrophages gradually increasing in number from day 7 to 1 month (Figs. 4D, 4G). The inflammatory cytokines IL6, IL10, IL1β, and tumor necrosis factor–α were significantly up-regulated in mouse OSA lacrimal gland tissue from days seven to 14, with a subsequent reduction thereafter to the one-month juncture (Fig. 4H). Similarly, protein expression of phosphorylated p65 was upregulated from day seven to day 14, with a mild decline thereafter (Figs. 4I, 4J). Collectively, the findings represent clear evidence of lacrimal gland inflammation in OSA mice. The production of reactive oxygen species (ROS) by OSA has been confirmed in multiple tissues.[37] Here, we observed alterations of oxidative stress in the lacrimal gland in the OSA model. The expression of oxidative stress marker NRF2 and SOD2 increased after modeling seven days, and gradually reduced from 14 days to one month (Figs. 4I, 4J).

Cellular Changes and Altered Expression of Hypoxia Inducible Factors in the Lacrimal Glands of OSA Mice

Myoepithelial cells in lacrimal glands are contractile, playing an important role in tear secretion.[38] They are also considered to be progenitors of acinar cells.[39] The αSMA is a marker of myoepithelial cells,[40] with immunostaining of mouse OSA lacrimal glands disclosing a gradual reduction in αSMA expression from day 7 to 1 month (Figs. 5A, 5D). Ki67-positive cells in lacrimal glands were few at day seven and remained low in number until one month (Fig. 5B). A qRT-PCR assay of Ki67 confirmed this result (Fig. 5E), with TUNEL assays showing that apoptotic cells gradually became more prevalent throughout the OSA period (Figs. 5C, 5F).

Because intermittent hypoxia is a characteristic of OSA,[37] we investigated classic hypoxia-inducible factors (*Hifs*) in the mouse OSA lacrimal gland. Immunostaining and qRT-PCR revealed a heightened expression of *Hif1*α at day seven of OSA. This change was transient, decreasing by day 14 and reverting to normal levels at one month (Figs. 6A, 6B).

Investigative Ophthalmology & Visual Science

Downloaded from intl.iovs.org on 04/19/2024

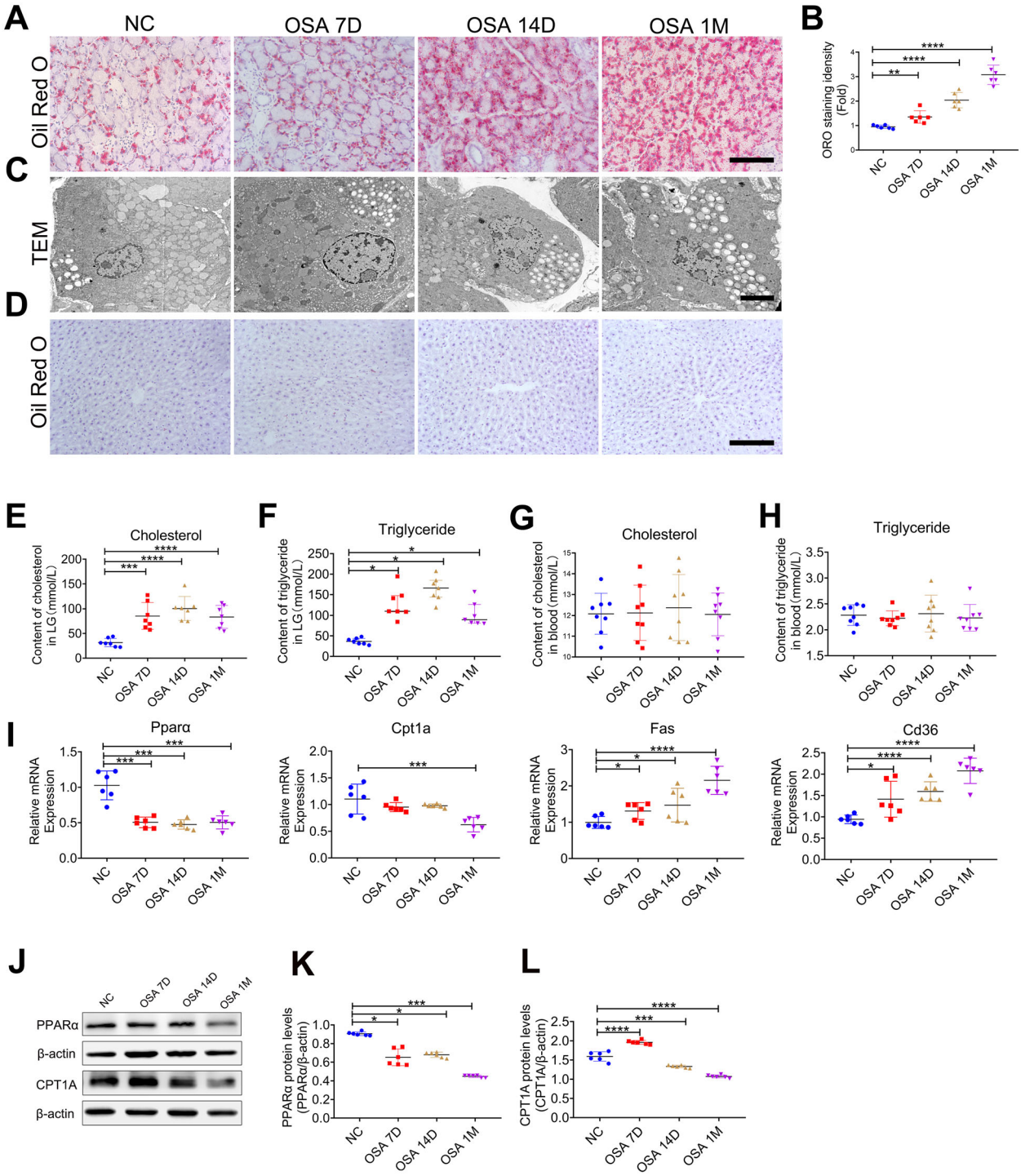

Figure 2. OSA induces abnormal lipid metabolism in lacrimal glands. (A) Oil red O staining reveals lipid deposition in OSA lacrimal glands. (B) The relative oil red O staining intensity shows lipid accumulation in OSA lacrimal glands. (C) Transmission electron microscopy identifies lipid droplets in OSA lacrimal gland acinar cells. (D) Oil red O staining reveals no lipid accumulation in the livers of mice after different durations of OSA. (E, F) Cholesterol and triglyceride levels, respectively, in OSA lacrimal glands. (G, H) Cholesterol and triglyceride levels in blood serum, respectively. (I) Gene expression of *Pparα, Cpt11a, Fas,* and *Cd36* in OSA lacrimal glands. (J) Western blot results indicate the protein expression of PPARα and CPT1A. Western blot quantification analysis of PPARα (K) and CPT1A (L). n = 6 (A–D, I–L); n = 7 (E and F); n = 8 (G and H). *$P < 0.05$, **$P < 0.01$, ***$P < 0.001$, ****$P < 0.0001$. *Scale bars*: 100 µm (A and D); 5 µm (C). D, day; M, month; NC, negative control.

The expression of *Hif2α* followed a similar trend (Figs. 6C, 6D), with Western blot analysis confirming the expression changes of *Hif1α* and *Hif2α* in OSA mouse lacrimal glands (Fig. 6E–G).

Investigative Ophthalmology & Visual Science

Downloaded from intl.iovs.org on 04/19/2024

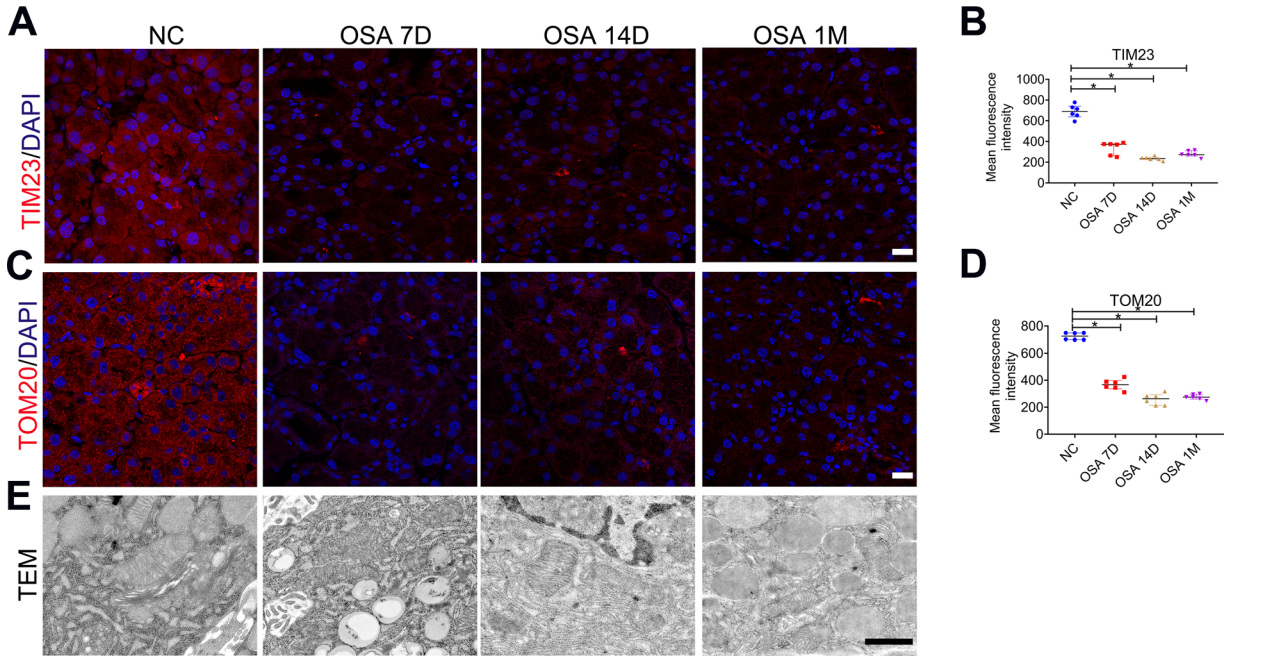

Figure 3. OSA affects the morphology and translocase expression of mitochondria in lacrimal glands. (A) Immunofluorescence staining of TIM23 (*red*) and DAPI (*blue*) in lacrimal glands. (B) Mean fluorescence intensity of TIM23 indicates a decreased expression of mitochondrial inner membrane protein in OSA lacrimal glands. (C) Immunofluorescence staining of TOM20 (*red*) and DAPI (*blue*). (D) Mean fluorescence intensity of TOM20 shows a decreased expression of mitochondrial outer membrane protein in OSA lacrimal glands. (E) Transmission electron microscopy reveals an altered microstructure of mitochondria in OSA lacrimal glands. n = 6 (A–E) *$P < 0.05$. *Scale bars*: 20 µm (A and C); 1 µm (E). D, day; M, month; NC, negative control.

Fenofibrate Alleviates Pathological Changes in Lacrimal Glands Induced by OSA

In the OSA mouse model, PPARα expression began to decrease at day seven and remained low thereafter (Fig. 2J). On this basis, we hypothesized that activation of the PPARα signaling pathway would be able to prevent lesions of the lacrimal gland induced by OSA. To test this idea, we fed OSA mice with fenofibrate, a *Pparα* agonist, from the start of OSA induction. This improved the condition of the corneal epithelium (Fig. 7A), with fluorescein staining scores further indicating that fenofibrate treatment alleviated the corneal epithelial defects from day seven to one month (Fig. 7B). Corneal sensitivity, moreover, recovered after feeding OSA mice with fenofibrate for one month (Fig. 7C). And body weight showed no significant change after feeding fenofibrate compared with the OSA group (Supplementary Fig. S1). Oil red O staining showed a significantly reduced accumulation of lipid in the lacrimal glands of OSA mice after one month of fenofibrate treatment (Figs. 7D, 7G), with transmission electron microscopy indicating a reduced prevalence of lipid droplets in lacrimal acinar cells (Fig. 7E). The tear secretion of OSA mice fed with fenofibrate was upregulated after two weeks, returning close to normal levels by one month (Fig. 7F). Fenofibrate also effectively reduced the amounts of cholesterol (Fig. 7H) and triglycerides (Fig. 7I) in the treated OSA lacrimal glands. Immunofluorescence staining of TOM20 (Figs. 7J, 7K) and TIM23 (Figs. 7L, 7M) revealed that the expression of mitochondrial functional proteins in OSA mice lacrimal glands was maintained with fenofibrate treatment, with transmission electron microscopy indicating a reduction in mitochondrial swelling as a consequence of fenofibrate treatment (Fig. 7N).

Fenofibrate was also found to diminish inflammation and apoptosis induced by OSA. This was evidenced by lower levels of cell infiltration in the OSA group with fenofibrate treatment (Figs. 8A, 8B), with CD4 positive lymphocytes (Fig. 8C, 8D), CD45 positive leukocytes (Figs. 8E, 8F) and F4/80 positive macrophages (Fig. 8G, 8H) less widespread. On the other hand, Ki67 expression was increased after fenofibrate treatment for one month in the OSA mouse (Figs. 8I, 8J), whereas the number of TUNEL positive cells was fewer (Figs. 8K, 8L). The expression of phosphorylated p65 was significantly downregulated in OSA mice lacrimal glands after one month of fenofibrate treatment (Figs. 8M, 8N). Besides, the expression of NRF2 and SOD2 reduced after treatment (Figs. 8M, 8N), and the structural integrity of myoepithelial cells was improved (Figs. 9A, 9B). The expression of HIF1α (Figs. 9C, 9D) and HIF2α (Figs. 9E, 9F) was also found to be upregulated in OSA lacrimal glands after fenofibrate treatment for one month. Put together, our results suggested that fenofibrate treatment could alleviate pathological changes in lacrimal glands induced by OSA.

Discussion

OSA can lead to multisystem abnormalities, such as nonalcoholic fatty liver disease,[41] dementia[42] and cardiovascular disease.[43] The current study shows that experimental OSA in mice activates the *Hif-Pparα* signaling axis by inducing intermittent hypoxia, further triggering a series of pathological changes that include abnormal lacrimal gland lipid metabolism and inflammatory cell infiltration, which ultimately leads to decreased aqueous tear secretion and dry eye-like changes in the ocular surface.

Investigative Ophthalmology & Visual Science

Downloaded from intl.iovs.org on 04/19/2024

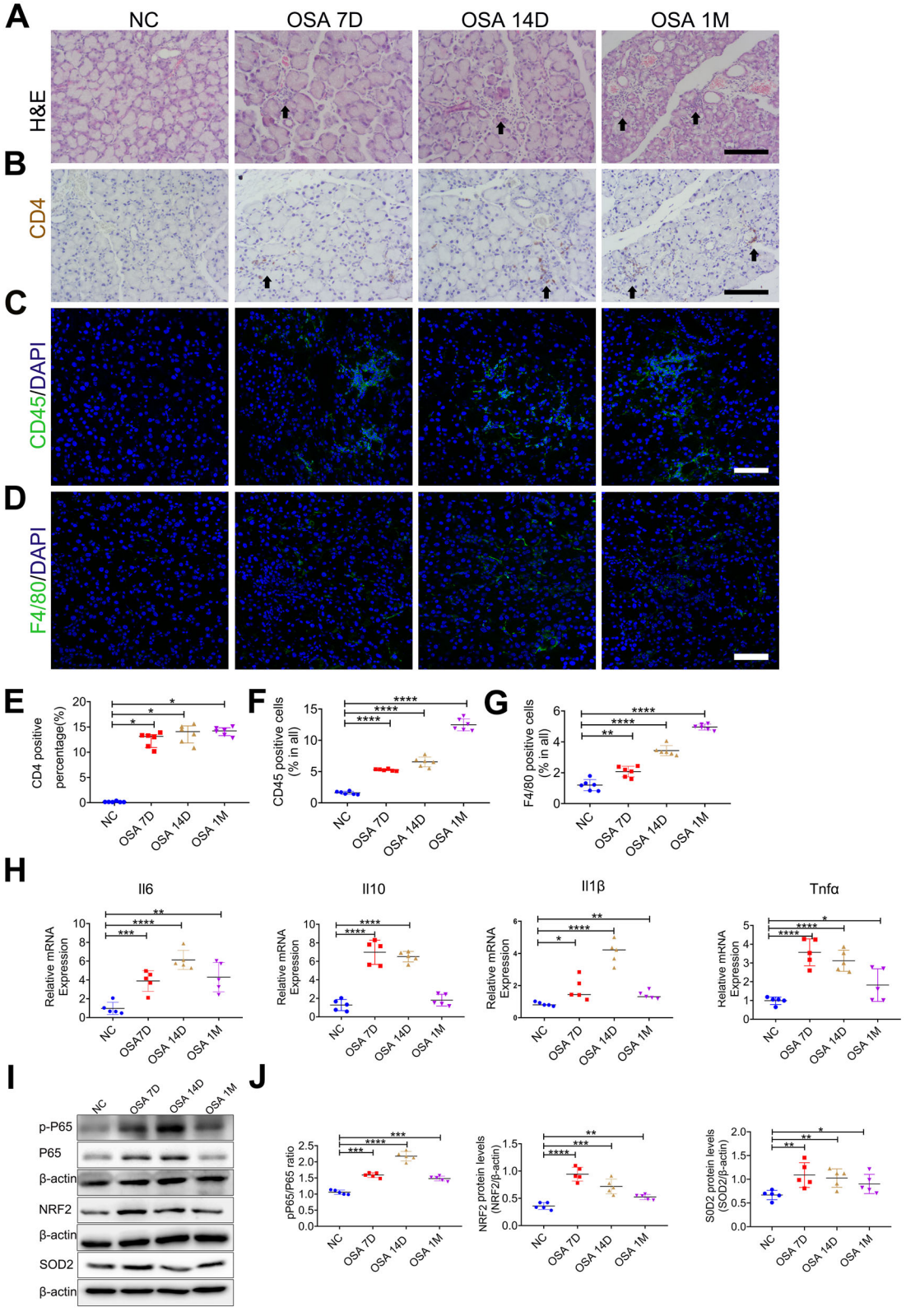

Figure 4. OSA induces inflammation in OSA lacrimal glands. (A) Hematoxylin and eosin staining reveals cellular infiltration in OSA lacrimal glands. *Black arrows* represent cellular infiltration. (B) Immunohistochemical staining demonstrates CD4 T lymphocytes. *Black arrows* represent positively stained areas. (C) Immunofluorescence staining of CD45 (*green*) shows the distribution of leukocytes (*blue*, DAPI). (D) Immunofluorescence staining of F4/80 (*green*) reveals macrophages in the OSA lacrimal gland (*blue*, DAPI). (E) Immunohistochemistry scores show that CD4-positive cells increase. Graphs show the specific counts of positive cells by CD45 (F) and F4/80 (G) staining. (H) The qRT-PCR determines gene expression levels of *Il6*, *Il10*, *Il1β*, and *Tnfα*. (I) Western blot reveals proteins expression of the phosphorylated P65, total P65, NRF2, and SOD2in the lacrimal glands of OSA mice. (J) Western blot quantification analysis of p-P65/P65, NRF2 and SOD2. n = 5 (H–J); n = 6 (A–G). *Scale bars*: 100 µm (A and B); 40 µm (C and D). **P* < 0.05, ***P* < 0.01, ****P* <0 .001, *****P* < 0.0001. D, day; M, month; NC, negative control.

Investigative Ophthalmology & Visual Science

Downloaded from intl.iovs.org on 04/19/2024

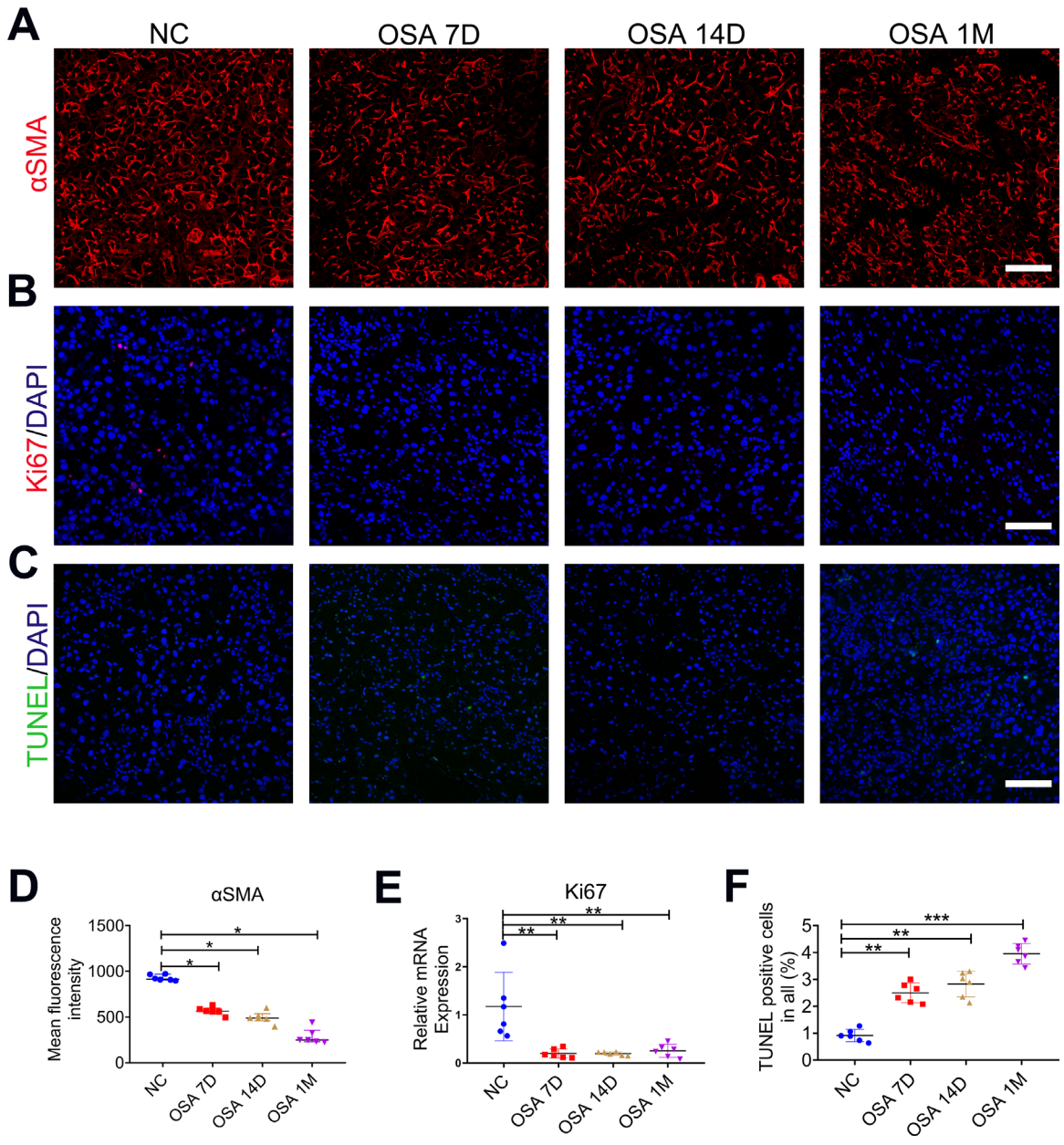

Figure 5. OSA affects proliferation, apoptosis and myoepithelial cell structure in OSA lacrimal glands. (A) Immunofluorescence staining of αSMA showing the distribution of myoepithelial cells. (B) Immunofluorescence staining of Ki67 (*red*) indicates proliferation of OSA lacrimal gland cells (*blue*, DAPI). (C) TUNEL staining (green) identifies apoptotic cells in OSA lacrimal glands (blue, DAPI). (D) Quantification of immunofluorescence staining for αSMA shows decreased expression of myoepithelial cell. (E) The qRT-PCR reveals the reduced expression of Ki67. (F) Graphs show the specific counts of positive cells by TUNEL staining. n = 6 (A-F). *Scale bars*: 40 µm (A–C). $^{*}P < 0.05$, $^{**}P < 0.01$, $^{***}P < 0.001$. D, day; M, month; NC, negative control.

Previous investigations have reported that hypoxia leads to lipid deposition in the liver, associated with the activation of *Hifα* under intermittent hypoxic conditions.[44] Hypoxia also triggers *Pparα* suppression through the activation of the *Hif2α* pathway in a steatotic human hepatocyte cell line and a mouse model of nonalcoholic fatty liver disease fed a high-fat diet, which eventually leads to abnormal lipid metabolism in the liver.[45] Data presented here reveal that OSA also leads to lipid deposition in the lacrimal gland. There was clear activation of HIF1α and HIF2α after subjecting mice to OSA-inducing conditions for seven to 14 days. Furthermore, the expression of *Hifα* downstream genes that are closely related to lipid metabolism such as *Pparα*, *Cpt1a*, *Fas* was altered, and the expression of *Cd36* was also changed. Here, we show that *Cd36* has a tendency to be upregulated, which may promote the uptake of lipid in lacrimal gland cells. Elevated *Fas* expression leads to increased intracellular endogenous lipids in lacrimal gland cells, whereas decreased *Cpt1a* expression causes limited intracellular fatty acid oxidation. Moreover, impaired mitochondrial function instigated by disruption of the inner and outer mitochondrial membranes can further exacerbate intracellular lipid deposition.[46] The above factors together could trigger lipid deposition in lacrimal gland cells. Previous studies have shown

Investigative Ophthalmology & Visual Science

Downloaded from intl.iovs.org on 04/19/2024

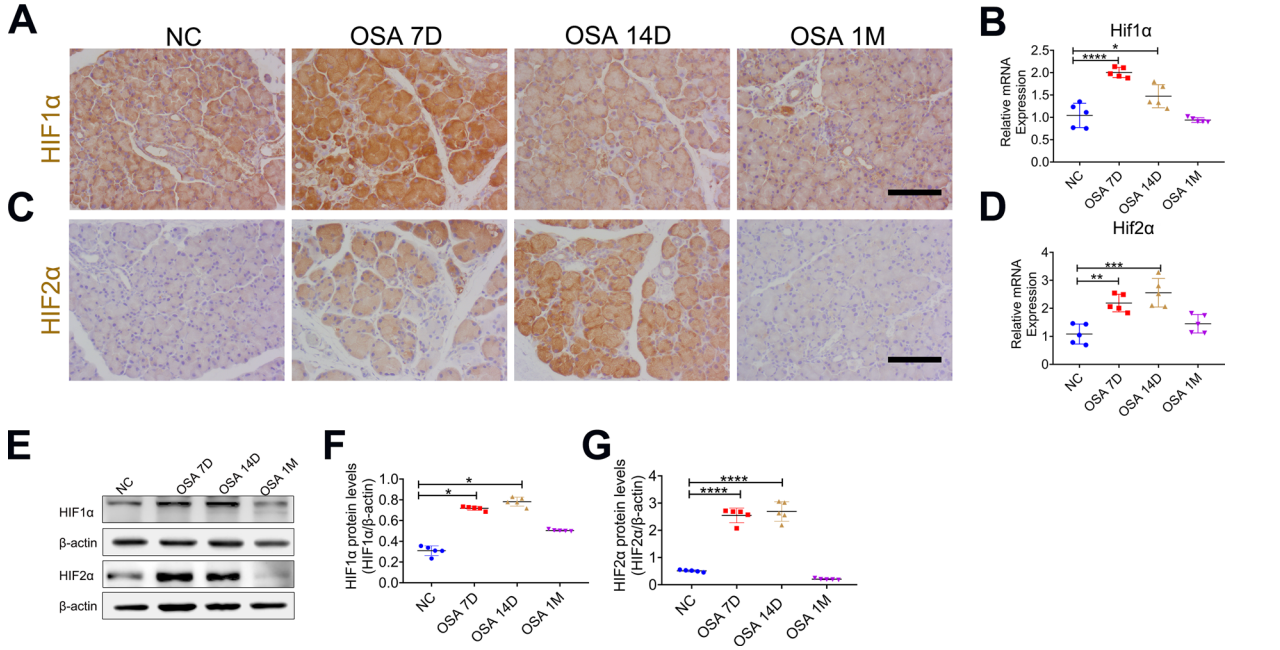

Figure 6. OSA induces hypoxia inducible factor changes in OSA lacrimal glands. (A, C) Immunohistochemical staining of HIF1α and HIF2α activation at different timepoints. (B, D) The qRT-PCR shows the gene expression of *Hif1α* and *Hif2α* in OSA lacrimal glands. (E) Western blot analysis indicates a change in the protein expression levels of HIF1α and HIF2α. (F, G) Western blot quantification analysis of HIF1α and HIF2α. n = 5 (A–G). *Scale bar*: 100 µm. *$P < 0.05$, **$P < 0.01$, ***$P < 0.001$, ****$P < 0.0001$. D, day; M, month; NC, negative control.

that six-month chronic intermittent hypoxia can induce lipid accumulation in the liver in a model of mice with diet-induced hepatic steatosis.[47] Interestingly, we found neither lipid deposition in the liver nor lipid changes in the blood serum under OSA conditions for one month. These results support the notion that the lacrimal gland may be a more sensitive organ than the liver to the effects of hypoxia and lipid metabolism.

Another significant change in OSA mice is the inflammation of the local microenvironment of the lacrimal gland. Under hypoxia the body initiates a complex and interrelated inflammatory cascade through HIF and NF-κB signaling pathways.[48] Previous reports have shown that OSA can activate the NF-κB signaling pathway, which in turn leads to the upregulation of its downstream inflammatory factors in murine macrophages injected with SARS-coronavirus or myeloid-restricted IkappaB Kinase (IKK)-β-deleted and *Hif1α* knockdown HK2 cells.[49–51] We also found activation of NF-κB signaling pathway in the lacrimal gland of OSA mice. Moreover, lipid deposition inside the acinar cells can cause lipid peroxidation, which induces an inflammatory response in lacrimal glands. Our previous study disclosed that lipid deposition led to inflammation in lacrimal glands of mice fed a high-fat diet.[27] Pericellular infiltrating inflammatory cells can also secrete inflammatory factors that affect the microenvironment of lacrimal gland cells and form an inflammatory cascade which modifies lacrimal gland function. Thus OSA-induced inflammation of the lacrimal gland is likely to be induced by a range of different mechanisms.

As a clinical sign of OSA, tear secretion in the experimental mice was found to be significantly reduced by day seven, which persisted until one month. Our previous studies reported that sleep deprivation[28] and a high-fat diet[27] also resulted in diminished tear secretion and lipid accumulation in lacrimal gland cells. This led to the conclusion that lipid deposition in lacrimal glands can disrupt their secretory functions. Inflammation of lacrimal glands under OSA conditions may also disturb secretion of lacrimal gland acinar cells.[52] This feature is shared with several diseases with lacrimal gland involvement and reduced tear secretion, such as Sjögren syndrome[53] and graft-versus-host disease.[54] Myoepithelial cells of the lacrimal gland were damaged in OSA mice. These cells exert pressure on acinar cells to secrete tears under neural regulation, and their damage can lead to a loss of extrusion function.[38,55] We also found that apoptotic cells were increased in the lacrimal glands of OSA mice, which may lead to loss of organ function.[56] *Hif,* moreover, leads to the disruption in mitochondria of the inner and outer membrane protein structure, suggesting intracellular hypoxia and impaired mitochondrial function.[57,58] The secretory function of the lacrimal gland is known to depend on the integrity of mitochondrial structure and function.[59,60] We propose that the combination of the factors described above cause the decreased tear secretion that is seen in the lacrimal glands of OSA mice.

Studies have shown that obese individuals are more likely to have OSA and that patients with OSA are at risk of obesity and metabolic syndromes.[43] Fenofibrate is one of the most widely used lipid-lowering drugs,[61,62] which can activate *Pparα*.[63,64] Our study found that OSA in experimental mice leads to lacrimal gland lipid deposition accompanied by *Pparα* downregulation. When fenofibrate was used to treat lacrimal gland pathological changes caused by OSA, we found upregulation of *Cpt1a* and downregulation of *Fas*, which is consistent with previous reports regarding the effect of fenofibrate. Interestingly, we found downregulation of *Cd36* expression in the lacrimal gland after fenofibrate treatment. Previous study revealed that *Pparα* agonist had no effect on *Cd36* expression in atherosclerosis model,[65] whereas other studies found that fenofibrate

Investigative Ophthalmology & Visual Science

Downloaded from intl.iovs.org on 04/19/2024

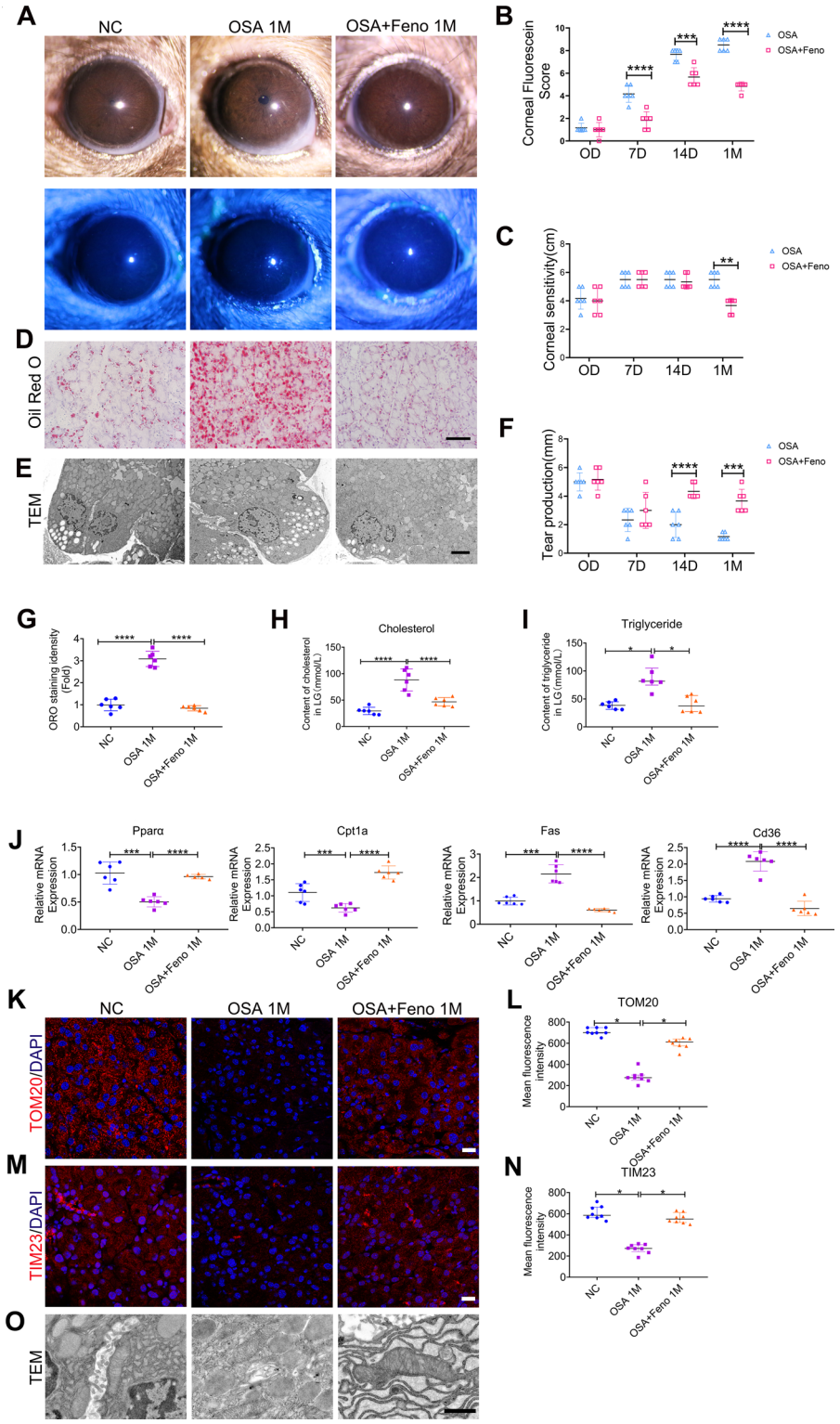

Figure 7. Fenofibrate reverses pathological changes in lacrimal glands induced by OSA. (A) Slit-lamp images show an improvement of the OSA-induced corneal epithelial defects after fenofibrate treatment. (B) Reduction of corneal epithelial defects identified by fluorescein staining scores. (C) Corneal sensitivity reverses to normal levels one month after fenofibrate treatment. (D) Oil red O staining reveals reduced lipid distribution in OSA lacrimal glands after fenofibrate treatment. (E) Transmission electron microscopy identifies lipid deposition in OSA lacrimal gland acinar cells. (F) Tear secretion values are increased after fenofibrate treatment. (G) Quantitation of oil red O staining reveals reduced lipid in lacrimal glands after fenofibrate treatment. (H) Cholesterol and (I) triglyceride levels in lacrimal glands are improved by fenofibrate. (J) The genes expression levels of *Pparα, Cpt1α, Fas* and *Cd36* were improved after fenofibrate treatment. (K) Immunofluorescence staining of TOM20 (*red*) is diminished in one-month OSA lacrimal glands but maintained with fenofibrate treatment. (L) Fluorescence quantification of TOM20 confirms the change. (M) TIM23 (*red*) immunostaining is reduced in one-month OSA lacrimal glands, whereas it is largely maintained with fenofibrate treatment. (N) Fluorescence quantification shows the recovery of TIM23. (O) Transmission electron microscopy shows a more integrated morphology in mitochondria in fenofibrate-feeding mice. n = 6 (A–J); n = 8 (K–N). *Scale bars*: 100 µm (D); 20 µm (J); 5 µm (E); 1 µm (N). **P* < 0.05, ***P* < 0.01, ****P* < 0.001, *****P* < 0.0001. D, day; M, month; NC, negative control.

Investigative Ophthalmology & Visual Science

Downloaded from intl.iovs.org on 04/19/2024

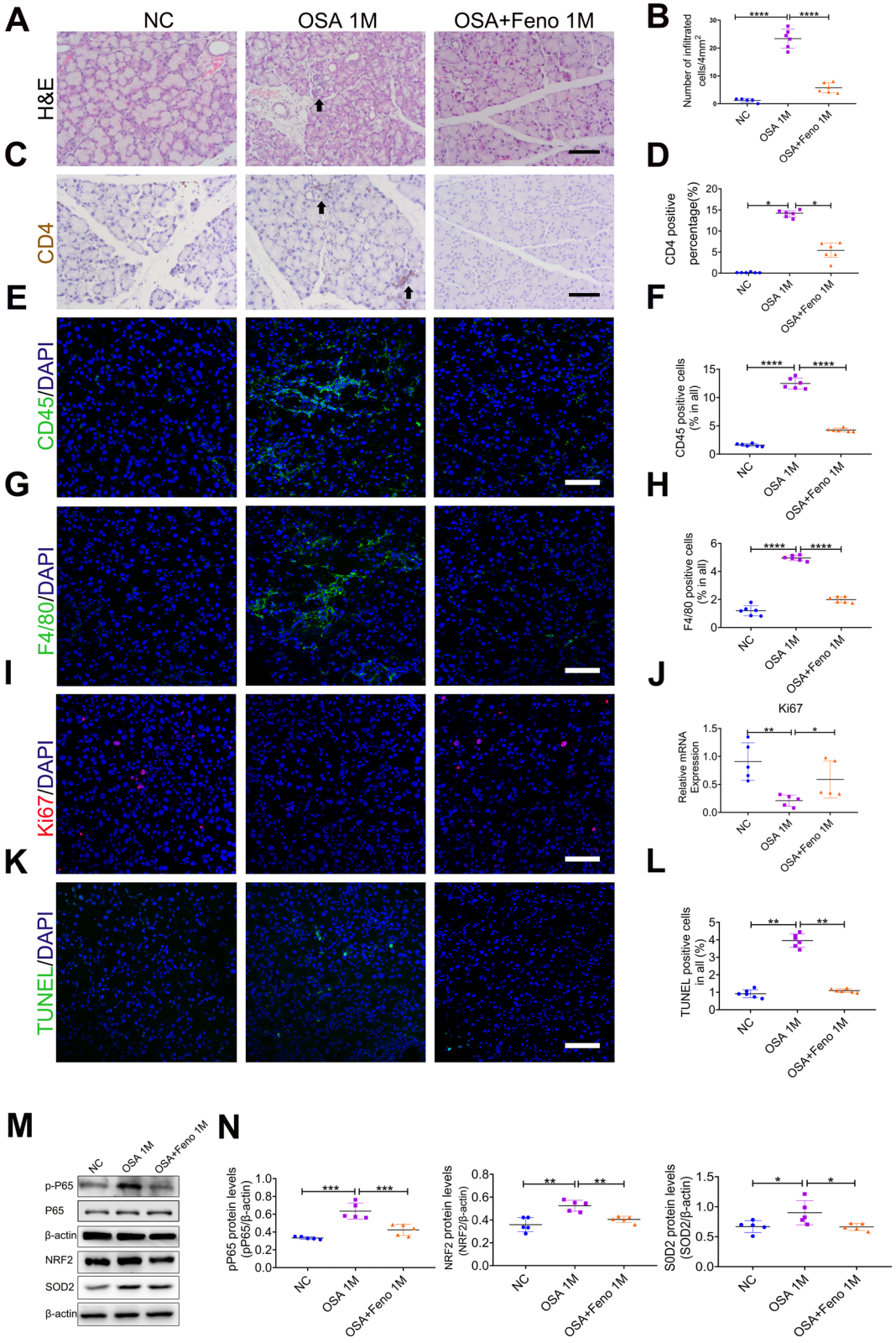

Figure 8. Fenofibrate ameliorates inflammation and apoptosis induced by OSA. (A) Hematoxylin and eosin staining of lacrimal glands reveals cellular infiltration (*black arrows*). (B) Counts of infiltrated cells shows decreased cellular infiltration after treatment with fenofibrate. (C) CD4 immuno-staining reveals positive T lymphocytes in lacrimal gland tissue. (D) CD4 immunohistochemistry scores reveal decreased CD4-positive staining after fenofibrate treatment. (E) CD45-positive leukocytes in OSA lacrimal glands are largely reduced after fenofibrate treatment. (F) Immunofluorescence intensity of CD45 confirms the change. (G) F4/80 positive macrophages show similar pattern as CD45. (H) Quantitative analysis of F4/80 staining also confirms a decrease of macrophages infiltration after fenofibrate treatment. (I, J) Immunofluorescence staining and RT-qCR of Ki67 reveal proliferation of lacrimal gland cells. (K) Apoptotic cells of the lacrimal gland, visualized by TUNEL staining are reduced after treatment. (L) Quantification of TUNEL staining reveals the intensity of apoptotic cells, which

Investigative Ophthalmology & Visual Science

Downloaded from intl.iovs.org on 04/19/2024

is decreased after treatment. (M) Western blot analysis indicates the change of total P65, phosphorylated p65, NRF2 and SOD2 in the lacrimal glands of OSA mice after treatment. (N) Western blot quantification analysis of p-P65/P65, NRF2 and SOD2. n = 5 (I, J, M, N); n = 6 (A–H, K–L). *Scale bars*: 100 µm (A and C); 40 µm (E, G, I and K). **P* <0 .05, ***P* < 0.01, ****P* < 0.001, *****P* < 0.0001. D, day; M, month; NC, negative control.

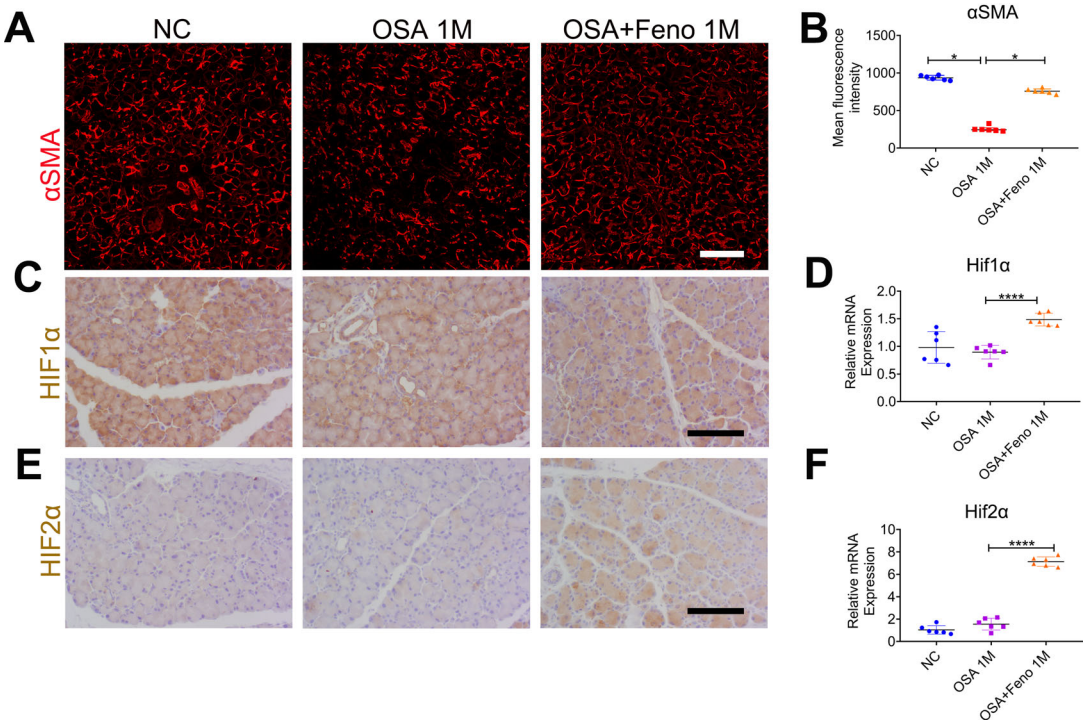

Figure 9. Fenofibrate restores myoepithelial cell structure and enhances the expression of hypoxia-inducible factors. (A) Immunofluorescence staining of αSMA indicates the expression of myoepithelial cells. (B) Quantification of αSMA staining reveals that fluorescence intensity decreased after one month of OSA induction, a change that was not seen after fenofibrate treatment. (C, E) Immunohistochemical staining of HIF1α and HIF2α shows an increased expression of HIF2α after fenofibrate treatment. (D, F) The qRT-PCR shows that the gene expression of *Hif1α* and *Hif2α* is increased after treatment with fenofibrate. n = 6 (A–F). *Scale bars*: 40 µm (A); 100 µm (C and E). **P* < 0 .05, *****P* < 0.0001. D, day; M, month; NC, negative control.

could increase *Cd36* gene expression in macrophages.[66] The inconsistency of our results from previous studies may be partially due to the dramatic decrease of infiltrated inflammatory cells in the lacrimal gland after fenofibrate treatment for one month, which may be the major contribution of *Cd36*. In our previous studies, we found that fenofibrate could restore mouse lacrimal gland dysfunction induced by a high-fat diet[27] and could restore sleep deficiency–triggered keratopathy.[67] Activation of *Pparα*, moreover, lessened the severity of mouse lacrimal gland lesions induced by sleep deficiency.[68] Clinical studies have also shown that fenofibrate can be used to improve the clinical symptoms of OSA by reducing blood lipid.[69] Fenofibrate also reduces inflammation in the retina and vascular endothelium,[70,71] whereas the activation of *Pparα* alleviates NF-κB phosphorylation.[72] Because of the complexity of the mechanism of fenofibrate on lipid metabolism, we believe its functional machinery on lacrimal gland deserves further research.

Hifs are the key regulators of oxygen homeostasis. They play a protective effect in ischemic cardiovascular disease, wound healing, and chronic rejection of organ transplants.[73] *Hif1α* can promote intestinal epithelium survival under hypoxia-related pathological conditions.[74] Activation of *Hif1α* can prevent dry eye–induced acinar cell death in the lacrimal gland,[75] *Hif1α* can also reduce the recruitment of inflammatory cells to lacrimal gland.[76] However, *Hifs* also go against retinal neovascularization, hereditary erythrocytosis and cancer.[73] Previous studies have disclosed tissue-specific and temporal alterations in *Hif* expression. Sacramento et al.[77] found that in a chronic intermittent hypoxia model, *Hif1α* and *Hif2α* expression did not show consistent trends over time in skeletal muscle, liver, and adipocytes. In the hypoxic cultured human L02 hepatocytes model, *HIF2α* increased after 12 hours, with the highest expression by 18 hours and gradually decreased after 24 hours, but *HIF1α* did not show any change.[78] In our study, we also found that HIF1α and HIF2α expression was upregulated at days seven and 14 of OSA and returned to normal control levels after 1 month. We speculate that the fluctuation of *Hifα* levels may be a consequence of the decompensation of lacrimal gland cell function after long-term hypoxia. Another interpretation is that lacrimal gland cells adapted to the chronic hypoxia environment, thus the *Hifα* expression levels dropped to normal level. Further study is mandatory to reveal the underlining mechanism. After the application of fenofibrate, the expression of *Hif1α* and *Hif2α* was upregulated significantly, suggesting that fenofibrate may help restore the compensation status of lacrimal gland

Investigative Ophthalmology & Visual Science

Downloaded from intl.iovs.org on 04/19/2024

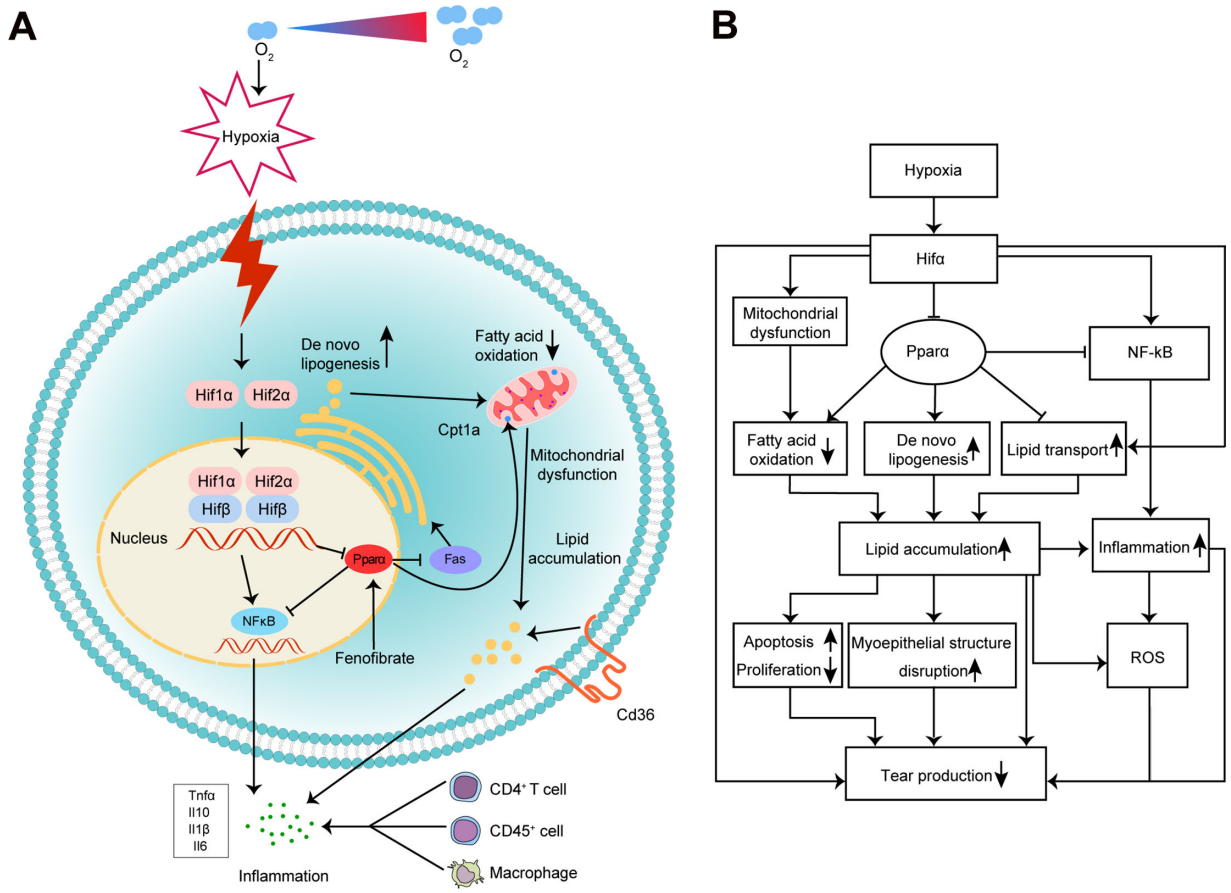

Figure 10. A proposed model of the *Hifα/Pparα* signaling axis induced by OSA (A) and a flow-chart of changes in lacrimal gland function (B). Chronic intermittent hypoxia induces an increase in *Hifα* expression in lacrimal gland cells. *Hifα* then translocates into the nucleus, combines with *Hifβ*, and activates downstream genes. *Hif* can inhibit *Pparα*, which leads to an increased intracellular lipid production via the regulation of *Fas* and a decrease in fatty acid oxidation via the regulation of *Cpt1a*. Upregulation of *Cd36* promotes the uptake of lipid in lacrimal gland. In addition, *Hifα* can activate the NF-κB signaling pathway, directly or indirectly through *Pparα*. Activation of the NF-κB signaling pathway, intracellular lipid deposition, and inflammatory cell infiltration contribute to inflammation in the lacrimal gland microenvironment. Lipid accumulation and inflammation could induce ROS production. Inflammation, lipid deposition, ROS, increased lacrimal gland apoptosis, mitochondrial dysfunction, and impaired myoepithelial structure ultimately lead to decreased aqueous tear production.

under a long-term intermittent hypoxia condition. Moreover, the abnormal accumulation of lipids in the lacrimal gland was reduced, and the function of lacrimal gland was maintained, indicating that fenofibrate may represent an effective therapy for the treatment of dry eye caused by OSA. It was reported that there is a mutual influence between *Hif* and NF-κB signaling pathways.[48] In our current study, we observed changes in *Hif* and NF-κB, whereas how the two signaling pathways interact with each other in the lacrimal gland under OSA condition still needs further exploration. In addition, *Hif* in inflammatory cells may be triggered by several factors such as intermittent hypoxia or inflammation.[79] The changes of *Hif* and NF-κB in inflammatory cells in OSA also need to be further investigated.

Oxidative stress plays an important role in the pathological changes of the lacrimal gland.[80–82] Here, we found that oxidative stress also occurs in the lacrimal gland in OSA model. The production of ROS by OSA has been found in multiple tissues.[37] Our recent study found that lipid deposition of the lacrimal gland can lead to oxidative stress.[83] Previous studies also found that hypoxia itself and secondary inflammation can lead to oxidative stress.[84,85] On the other hand, oxidative stress could activate inflammation,[86] which finally triggered a vicious cycle that led to an imbalance in the lacrimal gland microenvironment and decreased tear production.

In summary, we propose that OSA-induced hypoxia of the lacrimal gland can stimulate *Hif1α* and *Hif2α,* further activate the NF-κB signaling pathway, induce inflammation, and downregulate the *Pparα* signaling pathway. This results in abnormal lipid metabolism and mitochondrial dysfunction in lacrimal glands, induces lacrimal gland dyshomeostasis and ROS production, ultimately leading to a reduced aqueous tear secretion and the emergence of attendant dry eye pathological changes (Fig. 10). Fenofibrate treatment could inhibit NF-κB-related inflammation and reduce lipid accumulation in the lacrimal gland, thus ameliorating OSA-related dry eye syndrome. Our study for the first time confirmed causative relationship between OSA and lacrimal gland dysfunction and pointed out a potential clinical treatment for OSA-related dry eye.

Acknowledgments

Supported in part by the National Key R&D Program of China (No. 2018YFA0107301 [to WL], No. 2018YFA0107304 [to ZL]),

Investigative Ophthalmology & Visual Science

Downloaded from intl.iovs.org on 04/19/2024

the National Natural Science Foundation of China (NSFC, No. 81970773, No. 81770894, No. 81330022 [to WL], No. 81870627 [to ZL], No. 81870625 [to RZ]), Quanzhou High-level Talents Innovation Project (No. 2019C079R [to YG]). The funders have no role in the study design, data collection and analysis, decision on publishing, or preparation of the manuscript.

Disclosure: **S. Wang,** None; **X. He,** None; **Q. Li,** None; **Y. Zhang,** None; **J. Hu,** None; **R. Zong,** None; **J. Zhuang,** None; **A.J. Quantock,** None; **Y. Gao,** None; **W. Li,** None; **Z. Liu,** None

References

1. Jun JC, Chopra S, Schwartz AR. Sleep apnoea. *Eur Respir Rev*. 2016;25:12–18.
2. Benjafield AV, Ayas NT, Eastwood PR, et al. Estimation of the global prevalence and burden of obstructive sleep apnoea: a literature-based analysis. *Lancet Respir Med*. 2019;7:687–698.
3. Senaratna CV, Perret JL, Lodge CJ, et al. Prevalence of obstructive sleep apnea in the general population: a systematic review. *Sleep Med Rev*. 2017;34:70–81.
4. Economics DA. *Asleep on the job: Costs of inadequate sleep in Australia*. North Strathfield, Australia: Sleep Health Foundation; 2017.
5. Hillman DR, Murphy AS, Antic R, Pezzullo L. The economic cost of sleep disorders. *Sleep*. 2006;29:299–305.
6. Armeni P, Borsoi L, Donin G, Costa F, Ferini-Strambi L. PND33 the clinical and economic burden of obstructive sleep apnea in adults: A cost-of-illness analysis. *Value in Health*. 2019;22:S742.
7. Sullivan F. Hidden health crisis costing America billions: Underdiagnosing and undertreating obstructive sleep apnea draining healthcare system. *Am Acad Sleep Med*. 2016.
8. Gaisl T, Bratton DJ, Kohler M. The impact of obstructive sleep apnoea on the aorta. *Eur Respir J*. 2015;46:532–544.
9. Peppard PE, Young T, Palta M, Skatrud J. Prospective study of the association between sleep-disordered breathing and hypertension. *N Engl J Med*. 2000;342:1378–1384.
10. Rasche K, Keller T, Tautz B, et al. Obstructive sleep apnea and type 2 diabetes. *Eur J Med Res*. 2010;15:1–5.
11. Schröder CM, O'Hara R. Depression and obstructive sleep apnea (OSA). *Ann Gen Psychiatr*. 2005;4:1–8.
12. Jhuang Y-H, Chung C-H, Wang I-D, et al. Association of obstructive sleep apnea with the risk of male infertility in Taiwan. *JAMA Netw Open*. 2021;4:e2031846.
13. Yaggi HK, Concato J, Kernan WN, Lichtman JH, Brass LM, Mohsenin V. Obstructive sleep apnea as a risk factor for stroke and death. *N Engl J Med*. 2005;353:2034–2041.
14. Faridi O, Park SC, Liebmann JM, Ritch R. Glaucoma and obstructive sleep apnoea syndrome. *Clin Exp Ophthalmol*. 2012;40:408–419.
15. Agarwal R, Gupta SK, Agarwal P, Saxena R, Agrawal SS. Current concepts in the pathophysiology of glaucoma. *Indian J Ophthalmol*. 2009;57:257.
16. Muniesa MJ, Huerva V, Sánchez-de-la-Torre M, Martínez M, Jurjo C, Barbé F. The relationship between floppy eyelid syndrome and obstructive sleep apnoea. *Br J Ophthalmol*. 2013;97:1387–1390.
17. Sun M-H, Liao YJ, Lin C-C, Chiang RP-Y, Wei JC-C. Association between obstructive sleep apnea and optic neuropathy: a Taiwanese population-based cohort study. *Eye* 2018;32:1353–1358.
18. Palombi K, Renard E, Levy P, et al. Non-arteritic anterior ischaemic optic neuropathy is nearly systematically associated with obstructive sleep apnoea. *Br J Ophthalmol*. 2006;90:879–882.
19. Pellegrini M, Bernabei F, Friehmann A, Giannaccare G. Obstructive sleep apnea and keratoconus: a systematic review and meta-analysis. *Optom Vis Sci*. 2020;97:9–14.
20. Saidel MA, Paik JY, Garcia C, Russo P, Cao D, Bouchard C. Prevalence of sleep apnea syndrome and high-risk characteristics among keratoconus patients. *Cornea*. 2012;31:600–603.
21. Craig JP, Nichols KK, Akpek EK, et al. TFOS DEWS II definition and classification report. *Ocul Surf*. 2017;15:276–283.
22. Stapleton F, Alves M, Bunya VY, et al. TFOS DEWS II epidemiology report. *Ocul Surf*. 2017;15:334–365.
23. Karaca I, Yagci A, Palamar M, Tasbakan MS, Basoglu OK. Ocular surface assessment and morphological alterations in meibomian glands with meibography in obstructive sleep apnea Syndrome. *Ocul Surf*. 2019;17:771–776.
24. Lim E, Chee M, Sabanayagam C, et al. Relationship between sleep and symptoms of tear dysfunction in Singapore Malays and Indians. *Invest Ophthalmol Vis Sci*. 2019;60:1889–1897.
25. Zhang X, Qu Y, He X, et al. Dry eye management: targeting the ocular surface microenvironment. *Int J Mol Sci*. 2017;18:1398.
26. Jiao X, Lu D, Pei X, et al. Type 1 diabetes mellitus impairs diurnal oscillations in murine extraorbital lacrimal glands. *Ocul Surf*. 2020;18:438–452.
27. He X, Zhao Z, Wang S, et al. High-Fat Diet–Induced Functional and Pathologic Changes in Lacrimal Gland. *Am J Pathol*. 2020;190:2387–2402.
28. Li S, Ning K, Zhou J, et al. Sleep deprivation disrupts the lacrimal system and induces dry eye disease. *Exp Mol Med*. 2018;50:e451.
29. Wu K, Joffre C, Li X, et al. Altered expression of genes functioning in lipid homeostasis is associated with lipid deposition in NOD mouse lacrimal gland. *Exp Eye Res*. 2009;89:319–332.
30. Fletcher EC, Lesske J, Qian W, Miller CC, 3rd, Unger T. Repetitive, episodic hypoxia causes diurnal elevation of blood pressure in rats. *Hypertension*. 1992;19:555–561.
31. Soukhova-O'Hare GK, Shah ZA, Lei Z, Nozdrachev AD, Rao CV, Gozal D. Erectile dysfunction in a murine model of sleep apnea. *Am J Respir Crit Care Med*. 2008;178:644–650.
32. Zhao YS, An JR, Yang S, et al. Hydrogen and oxygen mixture to improve cardiac dysfunction and myocardial pathological changes induced by intermittent hypoxia in rats. *Oxid Med Cell Longev*. 2019;2019:7415212.
33. Livak KJ, Schmittgen TD. Analysis of relative gene expression data using real-time quantitative PCR and the 2− ΔΔCT method. *Methods*. 2001;25:402–408.
34. Kersten S, Stienstra R. The role and regulation of the peroxisome proliferator activated receptor alpha in human liver. *Biochimie*. 2017;136:75–84.
35. Bougarne N, Weyers B, Desmet SJ, et al. Molecular actions of PPARα in lipid metabolism and inflammation. *Endocr Rev*. 2018;39:760–802.
36. Kheirandish-Gozal L, Gozal D. Obstructive sleep apnea and inflammation: proof of concept based on two illustrative cytokines. *Int J Mol Sci*. 2019;20:459.
37. Prabhakar NR, Peng YJ, Nanduri J. Hypoxia-inducible factors and obstructive sleep apnea. *J Clin Invest*. 2020;130:5042–5051.
38. Makarenkova HP, Dartt DA. Myoepithelial cells: their origin and function in lacrimal gland morphogenesis, homeostasis, and repair. *Curr Mol Biol Rep*. 2015;1:115–123.
39. Shatos MA, Haugaard-Kedstrom L, Hodges RR, Dartt DA. Isolation and characterization of progenitor cells in uninjured, adult rat lacrimal gland. *Invest Ophthalmol Vis Sci*. 2012;53:2749–2759.
40. Lemullois M, Rossignol B, Mauduit P. Immunolocalization of myoepithelial cells in isolated acini of rat exorbital lacrimal

Investigative Ophthalmology & Visual Science

Downloaded from intl.iovs.org on 04/19/2024

gland: cellular distribution of muscarinic receptors. *Biol Cell*. 1996;86:175–181.

41. Mesarwi OA, Loomba R, Malhotra A. Obstructive sleep apnea, hypoxia, and nonalcoholic fatty liver disease. *Am J Respir Crit Care Med*. 2019;199:830–841.
42. Lutsey PL, Misialek JR, Mosley TH, et al. Sleep characteristics and risk of dementia and Alzheimer's disease: the atherosclerosis risk in communities study. *Alzheimers Dement*. 2018;14:157–166.
43. Drager LF, Togeiro SM, Polotsky VY, Lorenzi-Filho G. Obstructive sleep apnea: a cardiometabolic risk in obesity and the metabolic syndrome. *J Am Coll Cardiol*. 2013;62:569–576.
44. Mylonis I, Simos G, Paraskeva E. Hypoxia-inducible factors and the regulation of lipid metabolism. *Cells*. 2019;8:214.
45. Chen J, Chen J, Fu H, et al. Hypoxia exacerbates nonalcoholic fatty liver disease via the HIF-2α/PPARα pathway. *Am J Physiol Endocrinol Metab*. 2019;317(4):E710–E722.
46. Sangwung P, Petersen KF, Shulman GI, Knowles JW. Mitochondrial dysfunction, insulin resistance, and potential genetic implications. *Endocrinology*. 2020;161(4):bqaa017.
47. Savransky V, Bevans S, Nanayakkara A, et al. Chronic intermittent hypoxia causes hepatitis in a mouse model of diet-induced fatty liver. *Am J Physiol Gastrointest Liver Physiol*. 2007;293:G871–G877.
48. Cummins EP, Keogh CE, Crean D, Taylor CT. The role of HIF in immunity and inflammation. *Mol Aspects Med*. 2016;47-48:24–34.
49. Wang W, Ye L, Ye L, et al. Up-regulation of IL-6 and TNF-alpha induced by SARS-coronavirus spike protein in murine macrophages via NF-kappaB pathway. *Virus Res*. 2007;128:1–8.
50. Conde E, Giménez-Moyano S, Martín-Gómez L, et al. HIF-1α induction during reperfusion avoids maladaptive repair after renal ischemia/reperfusion involving miR127-3p. *Sci Rep*. 2017;7:41099.
51. Imamura T, Poulsen O, Haddad G. Intermittent hypoxia induces murine macrophage foam cell formation by IKK-β-dependent NF-κB pathway activation. *J Appl Physiol*. 2016;121:670–677.
52. Zoukhri D. Effect of inflammation on lacrimal gland function. *Exp Eye Res*. 2006;82:885–898.
53. Barr JY, Wang X, Meyerholz DK, Lieberman SM. CD8 T cells contribute to lacrimal gland pathology in the nonobese diabetic mouse model of Sjögren syndrome. *Immunol Cell Biol*. 2017;95:684–694.
54. Ogawa Y, Kuwana M, Yamazaki K, et al. Periductal area as the primary site for T-cell activation in lacrimal gland chronic graft-versus-host disease. *Invest Ophthalmol Vis Sci*. 2003;44:1888–1896.
55. García-Posadas L, Hodges RR, Utheim TP, et al. Lacrimal gland myoepithelial cells are altered in a mouse model of dry eye disease. *Am J Pathol*. 2020;190:2067–2079.
56. de Torres C, Munell F, Ferrer I, Reventós J, Macaya A. Identification of necrotic cell death by the TUNEL assay in the hypoxic-ischemic neonatal rat brain. *Neurosci Lett*. 1997;230:1–4.
57. Papandreou I, Cairns R, Fontana L, Lim A, Denko N. HIF-1 mediates adaptation to hypoxia by actively downregulating mitochondrial oxygen consumption. *Cell Metab*. 2006;3:187–197.
58. Zhang H, Bosch-Marce M, Shimoda L, et al. Mitochondrial autophagy is an HIF-1-dependent adaptive metabolic response to hypoxia. *J Biol Chem*. 2008;283:10892–10903.
59. Kotliarova A, Merlavs' kyĭ V, Dorosh O, Man'ko V. The role of mitochondrial uniporter in calcium-homeostasis of the exorbital lacrimal gland secretory cells. *Fiziolohichnyi Zhurnal (Kiev, Ukraine: 1994)*. 2014;60:73–81.
60. Bhattacharya S, García-Posadas L, Hodges RR, Makarenkova HP, Masli S, Dartt DA. Alteration in nerves and neurotransmitter stimulation of lacrimal gland secretion in the TSP-1(-/-) mouse model of aqueous deficiency dry eye. *Mucosal Immunol*. 2018;11:1138–1148.
61. Roberts W. Safety of fenofibrate—US and worldwide experience. *Cardiology*. 1989;76:169–179.
62. Derosa G, Sahebkar A, Maffioli P. The role of various peroxisome proliferator-activated receptors and their ligands in clinical practice. *J Cell Physiol*. 2018;233:153–161.
63. Badiou S, Merle De Boever C, Dupuy A, Baillat V, Cristol J, Reynes J. Fenofibrate improves the atherogenic lipid profile and enhances LDL resistance to oxidation in HIV-positive adults. *Atherosclerosis*. 2004;172:273–279.
64. Ferreira AVM, Parreira GG, Green A, Botion LM. Effects of fenofibrate on lipid metabolism in adipose tissue of rats. *Metabolism*. 2006;55:731–735.
65. Wu X, Cheng B, Guo X, Wu Q, Sun S, He P. PPARα/γ signaling pathways are involved in *Chlamydia pneumoniae*-induced foam cell formation via upregulation of SR-A1 and ACAT1 and downregulation of ABCA1/G1. *Microb Pathog*. 2021;161:105284.
66. Barbieri M, Di Filippo C, Esposito A, et al. Effects of PPARs agonists on cardiac metabolism in littermate and cardiomyocyte-specific PPAR-γ-knockout (CM-PGKO) mice. *PLoS One*. 2012;7:e35999.
67. Tang L, Wang X, Wu J, et al. Sleep deprivation induces dry eye through inhibition of PPARα expression in corneal epithelium. *Invest Ophthalmol Vis Sci*. 2018;59:5494–5508.
68. Chen Q, Ji C, Zheng R, et al. N-Palmitoylethanolamine maintains local lipid homeostasis to relieve sleep deprivation-induced dry eye syndrome. *Front Pharmacol*. 2019;10:1622.
69. Bruckert E, Duchêne E, Bonnefont-Rousselot D, et al. Proof of concept study: does fenofibrate have a role in sleep apnoea syndrome? *Curr Med Res Opin*. 2010;26:1185–1192.
70. Liu Q, Zhang F, Zhang X, et al. Fenofibrate ameliorates diabetic retinopathy by modulating Nrf2 signaling and NLRP3 inflammasome activation. *Mol Cell Biochem*. 2018;445:105–115.
71. Tomizawa A, Hattori Y, Inoue T, Hattori S, Kasai K. Fenofibrate suppresses microvascular inflammation and apoptosis through adenosine monophosphate–activated protein kinase activation. *Metabolism*. 2011;60:513–522.
72. Jain MR, Giri SR, Bhoi B, et al. Dual PPARα/γ agonist saroglitazar improves liver histopathology and biochemistry in experimental NASH models. *Liver Int*. 2018;38:1084–1094.
73. Semenza GL. Oxygen sensing, hypoxia-inducible factors, and disease pathophysiology. *Annu Rev Pathol*. 2014;9:47–71.
74. Karhausen J, Furuta GT, Tomaszewski JE, Johnson RS, Colgan SP, Haase VH. Epithelial hypoxia-inducible factor-1 is protective in murine experimental colitis. *J Clin Invest*. 2004;114:1098–1106.
75. Seo Y, Ji YW, Lee SM, et al. Activation of HIF-1α (hypoxia inducible factor-1α) prevents dry eye-induced acinar cell death in the lacrimal gland. *Cell Death Dis*. 2014;5:e1309.
76. Ji YW, Lee JH, Choi EY, et al. HIF1α-mediated TRAIL Expression Regulates Lacrimal Gland Inflammation in Dry Eye Disease. *Invest Ophthalmol Vis Sci*. 2020;61:3.
77. Sacramento JF, Ribeiro MJ, Rodrigues T, et al. Insulin resistance is associated with tissue-specific regulation of HIF-1α and HIF-2α during mild chronic intermittent hypoxia. *Respir Physiol Neurobiol*. 2016;228:30–38.
78. Chen J, Chen J, Fu H, et al. Hypoxia exacerbates nonalcoholic fatty liver disease via the HIF-2α/PPARα pathway. *Am J Physiol Endocrinol Metab*. 2019;317:E710–e722.

Investigative Ophthalmology & Visual Science

Downloaded from intl.iovs.org on 04/19/2024

79. Palazon A, Goldrath AW, Nizet V, Johnson RS. HIF transcription factors, inflammation, and immunity. *Immunity*. 2014;41:518–528.
80. Kojima T, Wakamatsu TH, Dogru M, et al. Age-related dysfunction of the lacrimal gland and oxidative stress: evidence from the Cu,Zn-superoxide dismutase-1 (Sod1) knockout mice. *Am J Pathol*. 2012;180:1879–1896.
81. Higuchi A, Ito K, Dogru M, et al. Corneal damage and lacrimal gland dysfunction in a smoking rat model. *Free Radic Biol Med*. 2011;51:2210–2216.
82. Kawashima M, Kawakita T, Okada N, et al. Calorie restriction: A new therapeutic intervention for age-related dry eye disease in rats. *Biochem Biophys Res Commun*. 2010;397:724–728.
83. He X, Zhao Z, Wang S, et al. High-Fat Diet-Induced Functional and Pathologic Changes in Lacrimal Gland. *Am J Pathol*. 2020;190:2387–2402.
84. Fuhrmann DC, Brüne B. Mitochondrial composition and function under the control of hypoxia. *Redox Biol*. 2017;12:208–215.
85. Mittal M, Siddiqui MR, Tran K, Reddy SP, Malik AB. Reactive oxygen species in inflammation and tissue injury. *Antioxid Redox Signal*. 2014;20:1126–1167.
86. Uchino Y, Kawakita T, Miyazawa M, et al. Oxidative stress induced inflammation initiates functional decline of tear production. *PLoS One*. 2012;7:e45805.

Investigative Ophthalmology & Visual Science

Downloaded from intl.iovs.org on 04/19/2024